

# High-resolution Integrated Micro-gyroscope for Space Applications

Hongwei Qu<sup>†</sup>, Deyou Fang<sup>†</sup>, Anwar Sadat<sup>‡</sup>, Peter Yuan<sup>‡</sup>, Huikai Xie<sup>†</sup>

<sup>†</sup>Department of Electrical & Computer Engineering, University of Florida, Gainesville, FL 32611

<sup>‡</sup>Department of Electrical & Computer Engineering, University of Central Florida, Orlando, Florida

## Abstract

In this paper, an integrated capacitive gyroscope fabricated by CMOS-MEMS technology is presented. The CMOS compatibility of the fabrication process enables full integration of the sensor with interface and signal conditioning circuitry on a single chip. The entire microstructure is single-crystal silicon based, resulting in large proof mass and good mechanical properties. Thus, high-resolution and high-robustness microgyroscopes can be obtained. With a resolution of about  $0.01^\circ/\text{s}/\text{Hz}^{1/2}$ , the fabricated gyroscope chip is only as small as 1.5mm by 2mm including the sensing elements and integrated electronics. The robustness, light weight and high performance make this type of MEMS gyroscope very suitable for space navigation applications where payload is critical. The on-chip capacitive sensing circuitry employs chopper stabilization technique to minimize the influence of  $1/f$  noise. The CMOS fabrication was performed through MOSIS by using the 4-metal TSMC  $0.35\mu\text{m}$  CMOS process. The post-CMOS micromachining processing consists of only dry etch steps and uses the interconnect metal layers as etching masks. Single-crystal silicon (SCS) structures are produced by applying a backside etch and forming a  $60\mu\text{m}$ -thick SCS membrane.

## 1. Introduction

Gyroscopes are devices which are used to measure angular rotation rate. Gyroscopes are widely used in airplanes, spacecrafts, missiles, automobiles and even consumer electronics. Traditional gyroscopes with spinning wheels employed in the present aerospace and military industries are bulky, need lubricant and eventually wear out. Ring laser gyroscopes (RLGs) are also expensive and heavy. A RLG typically weighs about 20 pounds (Fig. 1(a)).

### *Small size is critical*

MEMS gyroscopes are the perfect substitution, especially for micro-satellites and micro air vehicles due to their small size. They are suitable for long time flight because of low power consumption. Also, since they are light and low power consumption, an astronaut can wear several MEMS gyroscopes and accelerometers for positioning or monitoring his/her activities either in vehicle or out of vehicle during space travel. In fact, Robert Bosch Corporation started to sell MEMS gyroscopes for dynamic control of automobiles a few years ago [1]. Silicon Sensing Systems (SSS) is providing MEMS gyroscopes for

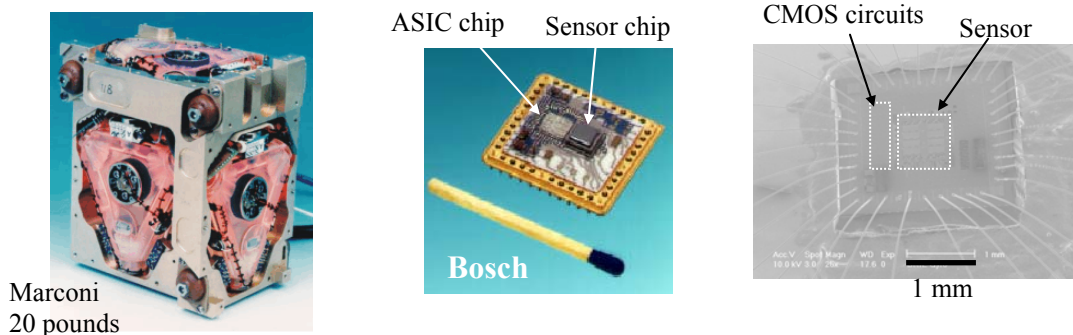


Figure 1: Different generations of gyroscopes: (a) Ring laser gyroscope; (b) Hybrid MEMS gyro (two-chip solution); and (c) Integrated MEMS gyroscope (one-chip solution).

Segway Human Transporters [2]. Analog Devices, Inc. (ADI) launched its first generation integrated MEMS gyroscopes in 2002 [3].

Silicon-based MEMS processes may be categorized into bulk micromachining and surface micromachining. A large mass is desired for a gyroscope because thermomechanical noise (Brownian noise) is inversely proportional to mass. Generally speaking, bulk micromachined gyroscopes have large mass and relatively large readout capacitance or piezoresistive readout. Therefore, most bulk micromachined gyroscopes do not incorporate on-chip read-out electronics, but instead require wire bonding to a separate electronic readout chips (a “two-chip” solution). Two-chip gyroscopes are expensive and have a relatively large package size that restricts their applications in consumer electronics regardless of price. In contrast, surface micromachining gyroscopes have small mass and relatively small readout capacitance. However, the sensors and read-out electronics are usually integrated on a single chip, to reduce parasitic capacitance.

Furthermore, most MEMS gyroscopes sense in only one axis, but angular rate is indeed a vector. Measuring all three-axis rotations is often required. Therefore, assembling three gyroscopes together is needed, which will greatly increase the package size, the complexity of packaging and the cost. A commercially available MEMS-based gyroscope made by Crossbow Technologies, Inc. measures 76mm x 95mm x 81mm and weighs about 1.4 pounds. It is much smaller than a RLG, but is still too large and heavy for many applications such as micro air vehicles.

### ***Integration is the solution***

There are three integrations required: i) electronics integration; ii) bulk/surface micromachining integration; and iii) multi-axis integration. With these three integrations, gyroscopes with high resolution, high robustness, low cost and small packaging size can be achieved.

Xie and Fedder already demonstrated a lateral-axis gyroscope with the first two integrations [4] by using a deep-reactive-ion-etch (DRIE) CMOS-MEMS process [5]. The unique DRIE CMOS-MEMS process takes advantage of the bulk micromachining's large mass as well as the surface micromachining's electronics integration. It is a maskless post-CMOS process and involves only dry-etch steps. A 0.8mm by 0.8mm lateral-axis gyroscope (see Fig. 1(c)), fabricated using the DRIE CMOS-MEMS process, achieved a noise floor of  $0.02^0/\text{sec}/\text{Hz}^{1/2}$  [4].

This paper reports a z-axis gyroscope fabricated by the same CMOS-MEMS process. Thus, combining with previously demonstrated lateral-axis gyroscopes, a monolithic 3-axis gyroscope device can be developed. The z-axis gyroscope structure will be similar to the one shown in Fig. 1(c). The chip containing three-axis gyroscopes will be about 3mm by 3mm in size. Signal conditioning and processing electronics can be integrated on the same chip. The final package will be only a quarter of the current single-axis Bosch gyroscope shown in Fig. 1(b). The fabrication process to make these devices is CMOS-compatible and can be easily transferred to high volume, automated, low cost CMOS production lines.

### ***Background on MEMS gyroscopes***

Draper Lab proposed the first silicon micromachined gyroscope in 1991 [6]. After that, various mechanisms, such as vibrating beams or rings, tuning forks, spinning disks, and surface-acoustic waves, were investigated for use in gyroscopes. Spinning gyroscopes have contact bearings, which pose a reliability problem. Surface-acoustic and fiber-optic gyroscopes require substantial process and materials development and integration. Among the various kinds of mechanisms, the suspended vibratory type, including tuning forks and vibrating beams or rings, is dominant because it is more suitable for batch fabrication in current micromachining processes. For example, there are electroplated metal ring structures [7], and polysilicon and single-crystal silicon ring structures [8]. The majority of MEMS gyroscopes use vibrating beam structures made of polysilicon structures [1,9,10], single-crystal silicon [11] or compound aluminum/silicon oxide structures [12].

## 2. DRIE CMOS-MEMS Process

In order to overcome some of the drawbacks of thin-film microstructures without losing the advantages of the multi-conductor structures, a new process sequence building on a previous post-CMOS micromachining process has been developed [5]. The basic idea is to introduce a single-crystal silicon (SCS) layer underneath the CMOS multi-layer structures in such a way that the mechanical properties are dominated by the SCS layer and electrical connections are provided by the CMOS microstructure layer. A diagram of the process flow is shown in Fig. 3. We start with a deep anisotropic backside etch leaving a 10 μm to 100 μm-thick SCS membrane (Fig. 3(a)). This backside etch step is used to control the thickness of microstructures. The cavity formed by the backside etch allows the completed die to be bonded directly to a package without interference from the released microstructures. Next, an anisotropic dielectric etch is performed from the front side (Fig. 3(b)). Then, in contrast to the prior work on post-CMOS processing, an anisotropic instead of an isotropic silicon etch is used for release (Fig. 3(c)). A thick, stiff, SCS layer remains underneath the CMOS layer, resulting in a relatively flat released microstructure, especially when compared with multi-layer thin-film CMOS-MEMS structures. Finally, a timed isotropic Si etch may be performed (Fig. 3(d)). This step provides a specific undercut of bulk Si to achieve electrical isolation of single-crystal silicon.

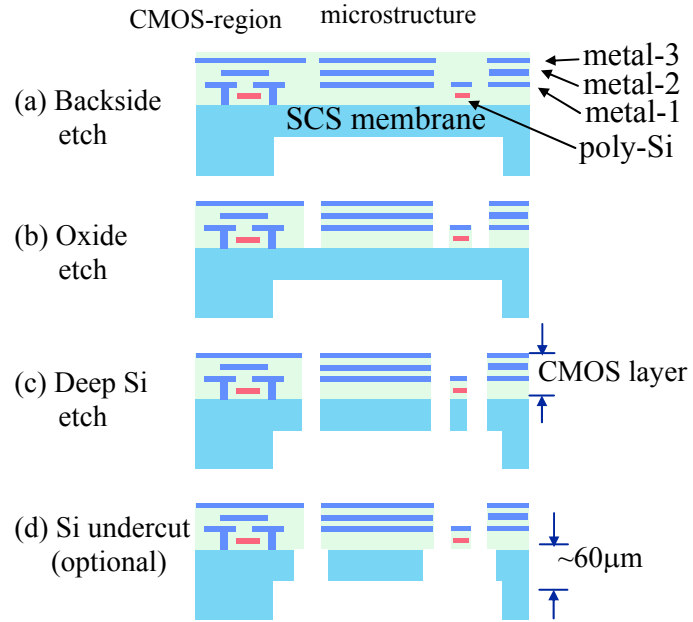


Figure 3. Cross-sectional view of DRIE CMOS-MEMS process.

## 3. Z-axis Vibratory Gyroscope Design

Coriolis acceleration is proportional to the cross product of vibrating velocity and angular rate, i.e.,

$$\vec{a}_c = 2 \cdot \vec{v} \times \vec{\Omega} \quad (1)$$

This equation shows that orthogonal lateral-axis vibration and acceleration sensing are required to detect the z-axis rotation. Assume the structure vibrates in the x direction and the Coriolis acceleration is detected in the y direction. Then a z-axis gyroscope topology is designed as shown in Fig. 4. It basically consists of two parts: (i) an x-axis comb drive to excite the vibration, and (ii) a y-axis accelerometer to sense the induced Coriolis acceleration. Also included are the x- and y- axis position sensors to monitor the primary vibration and the secondary coupling motion. A y-axis comb drive is also integrated to compensate the coupling.

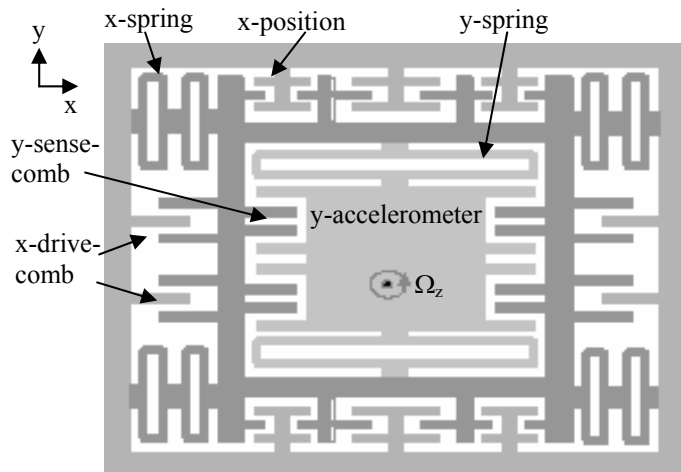


Figure 4. Topology of the proposed z-axis gyroscope.

**Behavioral Simulation**

A behavioral simulation tool based on Cadence/SpectreS has been developed by Qing and Fedder [13], which is called Nodal Design of Actuators and Sensors (NODAS). The basic components of the NODAS library include: beams (2D, 3D), plates (2D, 3D), comb drives (2D only) and splitters (2D to 3D adapter). These basic components can be used to build a complex system. Fig. 5(a) shows the NODAS representation of the z-axis gyroscope design shown in Fig. 4.

After the NODAS model for the z-axis gyroscope is built, the next step is to choose parameter values for each component. Comb-finger gap and spring-beam width are the two most critical parameters. Based on the past experience, the gap is set to 2.5 $\mu\text{m}$  and the spring-beam width is set to 6 $\mu\text{m}$ . The lengths of the drive springs and sense springs are 220 $\mu\text{m}$  and 200 $\mu\text{m}$ , respectively. The comb fingers are not included in this model just in order to simplify the model. The total area of the device is restricted to about 1mm by 1mm.

One of the major efforts to design a gyroscope is to achieve the desired mode allocation. Exactly matching the sense mode with the drive mode would generate maximum sensitivity. However it will limit the bandwidth and make the system very sensitive to any environmental variation or any mechanical creeping of the sensor. Since the gyroscope will operate in air, the mechanical Q-factor is small ( $\sim 20$ ). So our strategy is to shift the sense mode a little higher than the drive mode by tweaking the dimensional parameters of the components. The frequency and transient responses of NODAS simulation are shown in Fig. 5(b) and (c). The primary drive mode is 8.3 kHz, which is slightly lower than the sense mode which has a resonance frequency of 9.1 kHz. Also note that the phase difference between the excitation signal and the induced Coriolis motion.

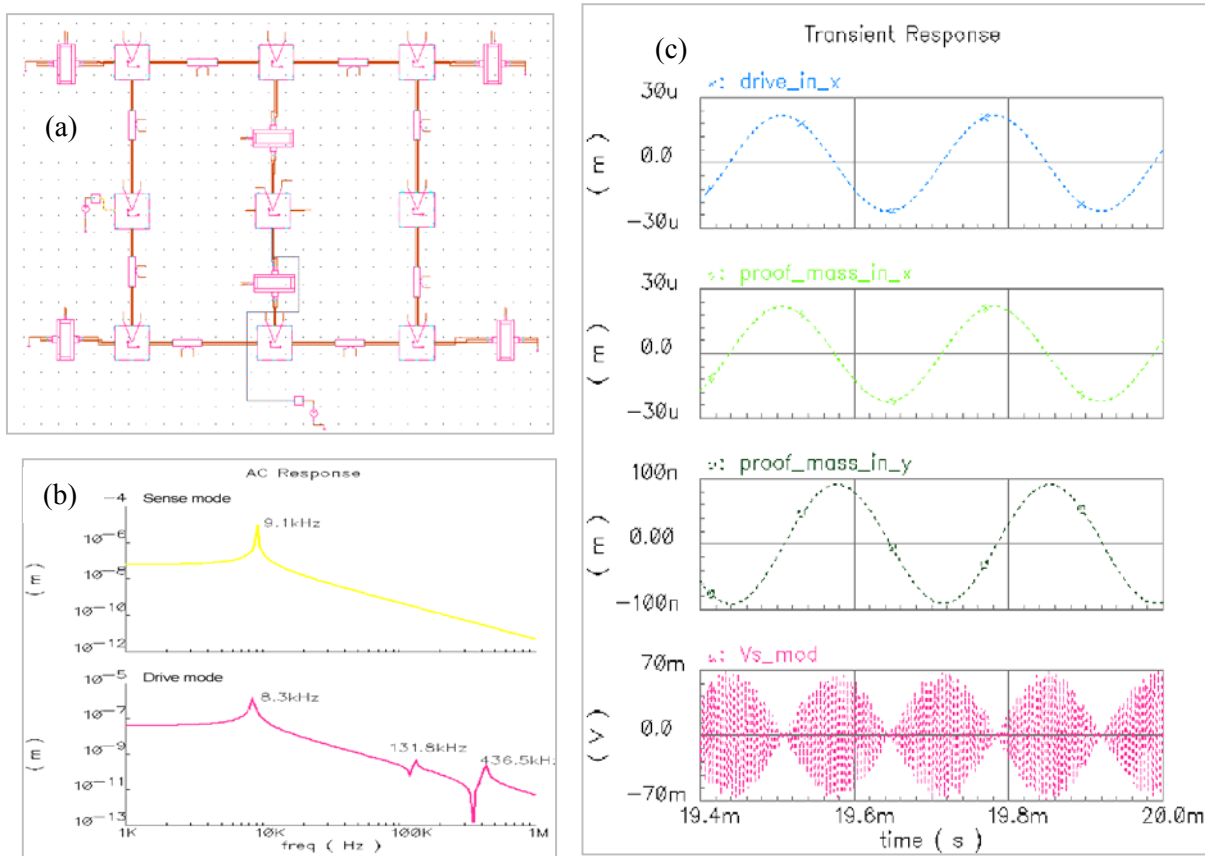


Figure 5. NODAS simulation results of the z-axis gyroscope. (a) NODAS model. (b) Frequency response. (c) Transient analysis.

#### 4. Circuits Design

The block diagram of the gyroscope system is shown in Fig. 6. Two interface circuits are integrated with the sensor on chip. One is a low-gain amplifier sensing the vibration of the drive mode. The other is a low-noise amplifier for picking up the Coriolis acceleration signal in the sensing mode. The vibration signal of the drive mode is fed back to the actuation comb drives to generate self oscillation. An off-chip amplifier is introduced to control the self-oscillation amplitude.

A CMOS continuous-time chopper stabilized amplifier, similar to [14], is used to amplify the Coriolis acceleration signal in the sensing mode. An open-loop, two-stage, fully differential amplifier topology is applied in this design. The schematic of the two-stage amplifier is shown in Fig. 7. The noise floor of the sensor is determined by both the thermomechanical noise of the sensing element and the CMOS circuits noise. The sensing signal will also be attenuated by the parasitic capacitance and the gate-to-ground capacitance of the input transistor of the first stage amplifier. To optimize the sensor noise performance, capacitance matching between the input stage of the amplifier and the sensing node is applied in the first stage design. Thus, a unity gain buffer between the sensor and the preamplifier is not needed, which eliminates the noise that would be introduced by the buffer otherwise. Robust d.c. biasing of the high impedance sensing nodes is provided by periodically resetting them to a d.c. level (i.e., switch biasing). In this design, the frequency of the dc reset clock is 1/16 of the modulation clock frequency, with a duty cycle of 1/16. Both modulation clock frequency and d.c. reset clock frequency are chosen to be much higher than the modulated sensing signal bandwidth to minimize signal distortion introduced by the switching d.c. biasing. Note that the rotational signal is modulated to the oscillation signal according to Eq. (1).

The d.c. offset of the amplifier is canceled by the d.c. feedback, which consists of a narrow-band amplifier and a large off-chip capacitor (>10nF). A passive demodulator and low-pass filter are then followed to obtain the base-band Coriolis signal. Due to process variations, there exists a sensor offset that introduces an a.c. signal to the amplifier, which will reduce the linear range or even saturate the amplifier. Thus, an auxiliary input pair is added in the second stage to cancel the a.c. signal resulted from the sensor offset. A second demodulation with the oscillation signal of driving mode followed by a second low-pass filter will yield the measuring rotational signal, as shown in Fig. 6.

The whole circuit layout was extracted and simulated in Cadence. With biasing currents of 1mA for the first stage and 4mA for the second stage of the differential amplifier, a gain of 47 dB and an input equivalent noise of  $4\text{nV}/\text{Hz}^{1/2}$  have been achieved. The 3 dB bandwidth is from 10 kHz to 9 MHz. The amplifier also achieves >30 dB cancellation of the circuit d.c. offset and >40 dB cancellation of the sensor offset.

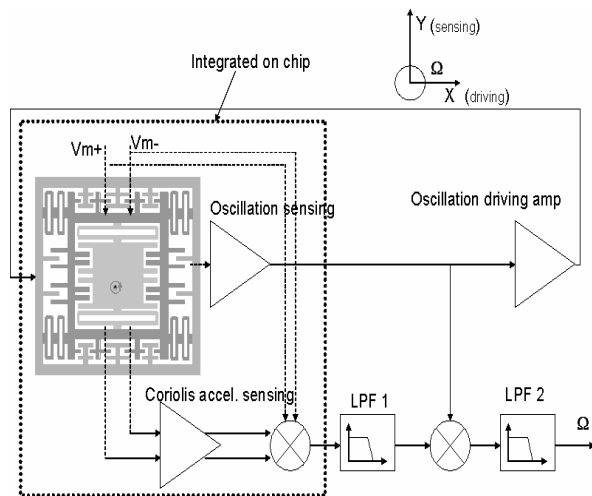


Figure 6. Block diagram of gyro system.

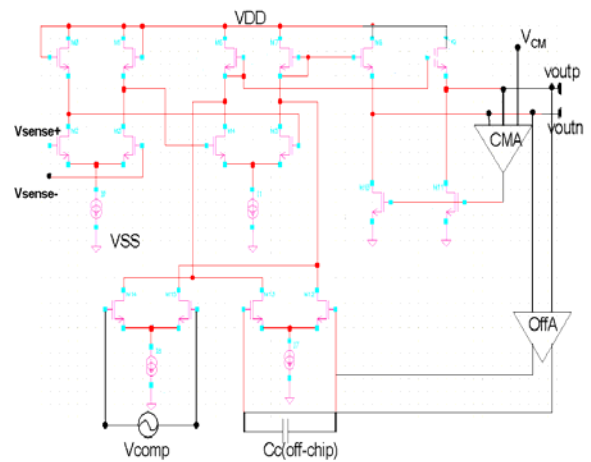


Figure 7. Schematic of the 2-stage differential amplifier.

## 5. Device Fabrication

The integrated gyroscope, including the interface circuits and sensing elements, is fabricated through MOSIS using TSMC 4-metal 0.35 $\mu\text{m}$  CMOS process before the sensor is released by the post-CMOS micromachining process shown in Fig. 3. The post-CMOS micromachining process consists of a set of anisotropic and isotropic dry etching steps. The last isotropic etch is employed to undercut silicon to form the electrical isolation of silicon. Fig. 6(a) shows the top view of the sensor element of the gyroscope.

A PlasmaTherm ECR (Electron Cyclotron Resonance) etcher was employed to conduct the thick  $\text{SiO}_2$  anisotropic etching. Since the maximum thickness of  $\text{SiO}_2$  is as thick as 7 $\mu\text{m}$  for the TSMC 0.35 $\mu\text{m}$  CMOS process [15], the ion milling effect on top aluminum layer and the undercutting of oxide are main concerns. The mixture of  $\text{CHF}_3$  and  $\text{O}_2$  was selected as the  $\text{SiO}_2$  etchant. The system pressure, coil and platen RF power and the gas flow were carefully optimized to guarantee a selectivity of 20 over aluminum etching. With a system pressure of 20mT, the  $\text{CHF}_3$  and  $\text{O}_2$  gas flow were calibrated to 30:20 sccm. The coil and platen power were 600W and 75W respectively.

Both the anisotropic and isotropic silicon etching were carried out on a STS DRIE system with  $\text{SF}_6$  as the reactive gas. The isotropic silicon etch is obtained by setting the platen RF power to zero. Since this isotropic etch undercuts silicon all over the structures, careful etching rate and timing control is required to avoid over-undercut the comb fingers. In addition, microloading effect (i.e., narrower gaps have lower etch rate) is used to reduce the silicon undercut of comb fingers as shown in Fig. 6(b) which shows the uniform and straight sidewall of the comb fingers.

The undercut of sensing comb fingers results in an increased gap between the comb fingers which will in turn decrease the sensitivity of the gyroscope. An advanced process is under development to overcome this undesired silicon undercut.

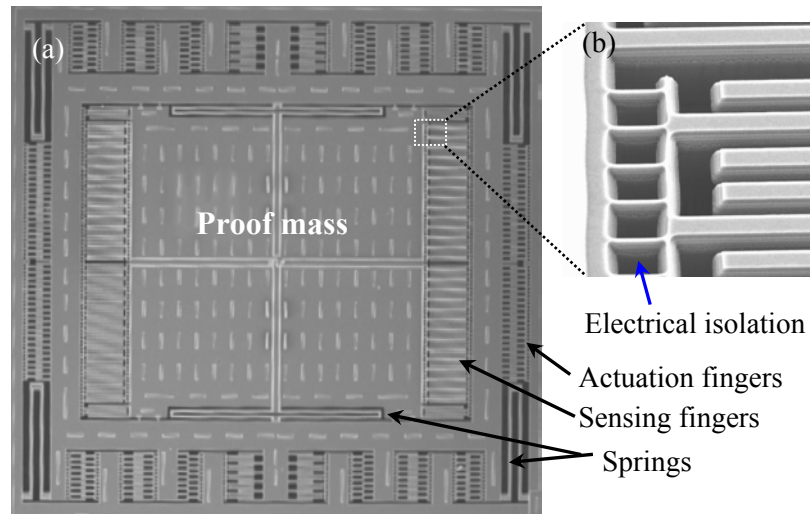


Fig.6. SEM image of released sensing element of the gyroscope. The inset shows the isolation structure connecting the sensing fingers and the proof mass. The bright stripes on the proof mass are slots required by TSMC 0.35 $\mu\text{m}$  technology to release the process stress.

## 6. Conclusions and Future Work

An integrated z-axis vibration gyroscope has been designed and fabricated based on TSMC 0.35- $\mu\text{m}$  CMOS technology. The post CMOS processes include anisotropic and isotropic dry etching of silicon and  $\text{SiO}_2$ , in which top layer metals act as the mask. Specific etching recipes have been developed to guarantee the performance of the sensor. The two-stage amplifier employs chopper-stabilization technique to reduce flicker noise. Simulation shows that the interface circuit provides a gain of 47 dB and an input equivalent noise of 4nV/Hz<sup>1/2</sup>. The circuit also achieves >30 dB cancellation of the circuit d.c. offset and >40 dB cancellation of the sensor offset. This vibration gyroscope is being tested and calibrated mechanically and electrically. An advanced post-CMOS micromachining process is under development to minimize the silicon undercut of comb fingers and springs.

## Acknowledgement

The project is supported by the NASA UCF/UF Space Research Initiative.

## References:

1. M. Lutz, W. Golderer, J. Gerstenmeier, J. Marek, B. Maihofer, S. Mahler, H. Munzel and U. Bischof, "A precision Yaw Rate Sensor in Silicon Micromachining", Transducers'97, Chicago, June 16-19, 1997, pp.847-850.
2. <http://www.baesystems.com/newsroom/2002/jul/220702news8.htm>.
3. <http://www.analog.com/technology/mems/gyroscopes>.
4. H. Xie, L. Erdmann, X. Zhu, K. Gabriel and G. Fedder, "Post-CMOS Processing For High-aspect-ratio Integrated Silicon Microstructures", Journal of Microelectromechanical Systems, vol.11, no.2, 2002, pp.93-101.
5. H. Xie, and G.K. Fedder, "Fabrication, characterization, and analysis of a DRIE CMOS-MEMS gyroscope," IEEE Sensors Journal, vol.3, no.5, Oct. 2003, pp. 622- 631.
6. P. Greiff, B. Boxenhorn, T. King, L. Niles, "Silicon monolithic micromechanical gyroscope", TRANSDUCERS '91, San Francisco, CA, USA; 24-27 June 1991, pp.966-968.
7. D. Sparks, D. Slaughter, R. Beni, L. Jordan, M. Chia, D. Rich, J. Johnson, T. Vas, "Chip-scale packaging of a gyroscope using wafer bonding", Sensors and Materials, vol.11, no.4, pp.197-207.
8. F. Ayazi, K. Najafi, "A HARPSS polysilicon vibrating ring gyroscope," Journal of Microelectromechanical Systems, vol. 10 (2001), pp. 169 –179.
9. J.A. Geen, S.J. Sherman, J.F. Chang and S.R. Lewis, "Single-chip surface-micromachining integrated gyroscope with 50 deg/hour root Allan variance", Digest of 2002 IEEE International Solid-State Circuits Conference, San Francisco, CA, Feb. 3-7, 2002, pp.426-427.
10. W.A. Clark, R.T. Howe, R. Horowitz, "Surface micromachined Z-axis vibratory rate gyroscope", Technical Digest. Solid-State Sensor and Actuator Workshop, Hilton Head Island, SC, USA; 3-6 June 1996, pp.283-287.
11. T.K. Tang, R.C. Gutierrez, C.B. Stell, V. Vorperian, G.A. Arakaki, J.T. Rice, W.J. Li, I. Chakraborty, K. Shcheglov, J.Z. Wilcox, W.J. Kaiser, "A packaged silicon MEMS vibratory gyroscope for microspacecraft", MEMS'97, Nagoya, Japan; 26-30 Jan. 1997, pp.500-505.
12. H. Xie, G. K. Fedder, "A CMOS-MEMS Lateral-axis Gyroscope", in The 14th IEEE International Conference on Micro Electro Mechanical Systems (MEMS 2001), Interlaken, Switzerland, January 21-25, 2001, pp.162-165.
13. Q. Jing and G. K. Fedder, NODAS 1.3 - Nodal Design Of Actuators And Sensors, in Proceedings of 1998 IEEE/VIUF International Workshop on Behavioral Modeling and Simulation (BMAS '98), October 26-28, 1998, Orlando, FL, USA.
14. J. Wu, G. K. Fedder, L. R. Carley, "A Low-Noise Low-Offset Chopper Stabilized Capacitive Readout Amplifier fro CMOS MEMS Accelerometers," IEEE Int. Solid- State Circuits Conf. Digest of Technical Papers, pp. 428-429, San Francisco, CA, 2002.
15. TSMC 0.35 $\mu$ m Mixed Signal Polycide 3.3V/5V Design Rules, T-035-MM-DR-001, Taiwan Semiconductor Manufacturing Company, Ltd, Rev.2.2.



**Hongwei Qu** received the B.S and M.S degree in electrical engineering both from Tianjin University, Tianjin, China in 1988 and 1993 respectively. From 1993 to 2000, he was a faculty member at the Electrical Engineering Department of Tianjin University, where he was involved in the research on semiconductor sensors. Mr. Qu is now pursuing the PhD degree at the Department of Electrical and Computer Engineering, University of Florida. Before he moved to University of Florida, he also obtained the M.S degree in physics from Florida International University in 2002, with thesis research on ferroelectric thin films. His current research involves CMOS MEMS technology, focusing on the integrated CMOS inertial measurement units. Mr. Qu is also interested in pressure, magnetic and other solid state sensors.



**Deyou Fang** received his M.S. in electrical and computer engineering from the University of Florida (UF), Gainesville, FL, in 2003, and now is pursuing his Ph.D. degree at UF. His research is focused on the design and implementation of integrated inertial sensors using CMOS-MEMS technology. After he got his B.S. in electrical engineering in 1993 from the University of Electronic Science and Technology of China, Chengdu, China, he worked on development of power station control systems for 3 years. In 1996, he joined Huawei Technologies Co. Ltd., where he spent 5 years on R&D of communication equipments, including telecommunication switches, GSM and CDMA2000 wireless systems and data communication systems.



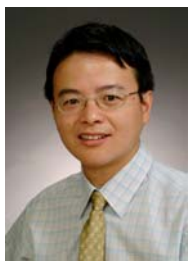
**Anwar Sadat** is a PhD candidate at the Department of Electrical and Computer Engineering of University of Central Florida (UCF). He received his MS in electrical engineering from UCF in 2001, and BS in electrical and electronic engineering from Bangladesh University of Engineering and Technology in 1996. From 1996 to 1999 he worked in Pacific Bangladesh Telecom Ltd., where he last hold the position of switch group leader. He is the chair for the IEEE ED/CPMT Orlando chapter. He received the Electrical Engineering Fellowship 2002 from UCF and Outstanding Graduate Student Award 2003 from IEEE Orlando section. His present research involves designing interface circuits for MEMS transducers. His research interests also include design and reliability analysis of analog, mixed signal and RF circuits.



**J.S. Peter Yuan** received both the M.S. and Ph.D. degrees (1984 and 1988) from the University of Florida. He joined the faculty at the University of Central Florida (UCF) in 1990 after one year of industrial experience at Texas Instruments, Inc., where he was involved with the 16-MB CMOS DRAM design. Currently, he is a Professor and Director of the Chip Design and Reliability Laboratory at UCF.

Dr. Yuan has published more than 180 papers in referred journals and conference proceedings in the area of semiconductor devices and circuits. He has authored the book *Semiconductor Device Physics and Simulation*, published by Plenum in 1998 and the book *SiGe, GaAs, and InP Heterojunction Bipolar Transistors* published by Wiley in 1999. Since 1990 he has conducted many research projects funded by NSF, Motorola, Harris, Lucent Technologies, National Semiconductor, and Theseus Logic. He serves regularly as a reviewer for the IEEE Transactions on Electron Devices, IEEE Electron Device Letters, and Solid-State Electronics. He has received many awards. These include the Research Incentive Award, UCF, 2003, the Distinguished Researcher Award, UCF, 2002, Outstanding Engineering Award, IEEE Orlando Section, 2002, TIP award, UCF, 1995, Outstanding Engineering Educator Award, IEEE Orlando Section and Florida Council, 1993. He is listed in *Who's Who in American Education* and *Who's Who in Science and Engineering*.

Dr. Yuan is a senior member of IEEE and member of Eta Kappa Nu and Tau Beta Pi. He is an Editor of the IEEE Transactions on Device and Materials Reliability.



**Huikai Xie** is an Assistant Professor at the Department of Electrical and Computer Engineering of the University of Florida. He received his MS in electro-optics from Tufts University in 1998, and PhD degree in electrical and computer engineering from Carnegie Mellon University in 2002. He also holds BS and MS degrees in electronic engineering from Beijing Institute of Technology. From 1992 to 1996, he was a faculty member of the Institute of Microelectronics at Tsinghua University, Beijing, working on various silicon-based chemical and mechanical sensors. He has published over 40 technical papers. His present research interests include micro/nanofabrication, integrated microsensors, gyroscopes, IMUs, optical MEMS and biophotonics.